Stator Current-Sensorless Modulated Model Predictive Direct Power Control of a DFIM with Magnetizing Characteristic Identification

Stator Current-Sensorless Modulated Model Predictive Direct Power Control of a DFIM with Magnetizing Characteristic Identification

Shafiq Odhano, *Senior Member, IEEE,* Sandro Rubino, *Member, IEEE,* Mi Tang, *Member, IEEE,* Pericle Zanchetta, *Fellow, IEEE,* Radu Bojoi, *Fellow, IEEE*

***Abstract*—The paper presents a direct power control method based on modulated model predictive control for a doubly fed induction machine. The modulated predictive control algorithm constructs an optimal voltage vector from two inverter states that give minimum absolute error in the active and reactive power. The paper focuses on the effects of magnetic saturation and its impact on the accuracy of computed reactive power when the stator current sensors are not installed. To reduce the impact of magnetic saturation on reactive power computation, the machine's magnetizing characteristic is identified through a self-commissioning scheme introduced in this paper. The identified magnetizing curve is utilized to construct a full-state stator flux observer which is used to accurately estimate stator currents that appear in the reactive power equation. Experimental results are presented to demonstrate the accuracy of the reactive power computation in the absence of stator current sensors while conserving the rapid transient response offered by a modulated predictive control strategy for active and reactive power regulation.**

***Index Terms*—direct power control, doubly fed induction machine, magnetic saturation, modulated model predictive control, reactive power control, wind power generation**

I. Introduction

Squirrel cage induction machines, with their fixed torque-speed characteristics, are a common occurrence in domestic and industrial applications [1]. Induction machines with three-phase windings on the rotor allow their torque-speed characteristic to be varied by changing the rotor resistance, these are mostly used in applications demanding high torque [2]. The wound rotor induction machines are also used in wind energy conversion systems where the stator is directly connected to the utility grid and the rotor windings are fed by a power electronic converter, hence the name doubly-fed induction machine (DFIM). This arrangement reduces the ratings of the power converter while at the same time permits the four-quadrant control of active and reactive power supplied to or absorbed from the grid. The control of DFIM has been the subject of research particularly with regards to the direct power control (DPC) [3]–[8].

Achieving DPC of a DFIM is similar [5] to implementing the direct self control i.e. direct torque and flux control [9]. However, as with the direct torque control, DPC also results in a variable switching frequency. The finite control set model predictive control (FCS-MPC) also leads to a non-constant switching frequency [10], [11] although some works [3], [4], [8] present modulator-based predictive control resulting in a fixed converter switching frequency.

As the DFIM stator is generally connected to the grid directly, the control needs to be robust against any disturbances in the grid conditions such as voltage imbalances as discussed in [11]. The active and reactive power references that are calculated based on the distorted grid voltage are not clean enough to allow harmonic-free currents being injected into the grid from the DFIM. In [11], the power references are modified by adding compensation terms to ensure that the DFIM supplies sinusoidal currents to the grid; besides, the modified power references achieve ripple-free torque on the wind turbine shaft. The negative implications of distorted grid voltage are also studied in [7] in which the phase locked loop (PLL) is replaced by a second-order vector integration. The harmonics in the grid voltage appear as unwanted oscillations in the angle estimated by a standard PLL. The vector integrator of [7] acts as a direct resonant controller to eliminate the low-order harmonics from the grid voltage such as the fifth and the seventh. A ripple-free grid voltage vector angle results in stable power references and sinusoidal currents in the machine minimizing shaft torque ripple. To track a varying grid frequency, [7] proposes an adaptive frequency detection scheme. Proportional-integral (PI) controllers are used to control active and reactive power. Compared to a standard PLL, the second-order vector integration has been shown to be robust against grid disturbances [7]. Among other sources of error in the DPC are parameter mismatches; these are addressed in [10] through the addition of a correction term in the reference rotor voltage calculated by a deadbeat action. The robust FCS-MPC algorithm of [10] starts by generating the rotor reference voltage using deadbeat current control. An additional voltage term to remove error due to parameter detuning is also computed. The resultant voltage reference is then compared with the voltage vectors associated with the seven inverter states thus allowing to define a cost function. The inverter

Manuscript received January 30, 2020; revised April 22 and August 5, 2020; accepted September 9, 2020

S. Odhano is with the School of Engineering, Newcastle University, Newcastle Upon Tyne NE1 7RU, U.K. (email: shafiq.odhano@newcastle.ac.uk)

S. Rubino and R. Bojoi are with Dipartimento Energia "G. Ferraris", Politecnico di Torino, Turin 10129, Italy (email: sandro.rubino@polito.it; radu.bojoi@polito.it)

M. Tang is with the Power Electronics, Machines and Control Group, University of Nottingham, Nottingham NG7 2RD, U.K. (email: mi.tang2@nottingham.ac.uk)

P. Zanchetta is with the Department of Electrical and Electronic Engineering, University of Nottingham, Nottingham NG7 2RD, U.K., and also with the Department of Electrical Computer, and Biomedical Engineering, University of Pavia, Pavia 27100, Italy (email: pericle.zanchetta@nottingham.ac.uk)

state that minimizes this cost function is chosen and applied during the next switching period. The switching frequency for the FCS-MPC power control [10] is not constant as in the DPC [11] with modified power references.

Prediction of stator active and reactive power is used in [4] and compared with the reference power values to calculate error terms. The rotor voltage vector to eliminate the active and reactive power errors is given directly by the rotor voltage equation. The voltage vector thus calculated is applied through a space vector modulation stage during the next switching period that results in a constant switching frequency. A scheme similar to [4] is proposed in [3] where grid synchronization is achieved through virtual torque control. The control action in [3] is computed following the principle used in [4] thus resembling a deadbeat control. However, different from [4] the control scheme of [3] is implemented without a rotor position sensor. DPC under unbalanced grid conditions and with constant switching frequency is also investigated in [8]. Using all the eight inverter switching states, the active and reactive power slopes are estimated and four switching states are selected based on the following two criteria: (i) states that minimize a cost function of power errors and (ii) have positive durations. The four selected states correspond to four voltage vectors, of which two are *necessarily* active vectors between which the stator flux vector lies and the other two are zero voltage vectors. The duty cycle with which to apply the active and zero vectors is calculated using the active and reactive power slopes, making the scheme resemble modulated MPC of [12]. Another work that deals with MPC application for DFIM is reported in [13] where the rotor side converter also includes LC filter. The current control is achieved through integral error feedback.

The research in the control of DFIM is not limited to prediction-based strategies only, other techniques such as sliding mode controller [6] have also been investigated. In [6], harmonics caused by grid imbalances are shown as additional terms in power references using *extended active power* concept. In the extended active power equation, the negative sequence components of grid voltage and current appear, which are removed through feed-forward compensation. This renders the power delivered by the DFIM to the grid consist of only positive sequence components of current and voltage. The control uses integral form sliding surface sliding mode controller to obtain decent steady state and transient power control performance. All the works discussed so far [3]–[8], [10], [11], [13] use two-level voltage source inverter (VSI) for DFIM control; however, [14] presented DFIM vector control with an indirect matrix converter that, by definition, has a non-constant dc-link voltage. The paper [14] demonstrated that fast power control with negligible steady-state error can still be achieved without using large dc-link capacitance as used in a VSI.

The aforementioned power control techniques do not consider errors or variations in machine parameters, except [10], and treat them as constants. If the temperature of the machine does not change substantially, the stator and rotor resistances do remain constant, apart from negligibly small variations caused by changes in the frequency. Similarly, the leakage inductances do not undergo significant changes during normal operation. However, the variations in magnetizing inductance caused by main flux saturation cannot be ignored. The literature reports some works that highlight magnetizing inductance variations such as [15], in which a model reference adaptive system based inductance estimation is proposed. It is observed that using an accurate value of magnetizing inductance renders the control robust particularly when position sensorless schemes are implemented [15]. Similarly, in [16] the effects of main flux saturation on the controllability of the DFIM are analysed through short-circuit modelling with particular attention to uninterrupted control under faults. Although [15], [16] have discussed the influence of magnetic saturation on control performance, the influence of magnetizing inductance variation on DPC is largely ignored in the literature. Besides, the methods for identifying the variations in main inductance are not widely covered.

Therefore, in this paper, a detailed analysis of how the reactive power estimation is affected by an inaccurate magnetizing inductance value is presented. The reactive power estimation accuracy in the absence of stator current sensors, or when the current sensing is unavailable due to a fault, heavily depends on how accurately the magnetizing inductance of the machine, at the particular operating point, is known. For these analyses, offline characterization tests are first conducted on the machine under test and a look-up table (LUT) is constructed for main inductance as a function of magnetizing current. This LUT is then used inside a full-state flux observer to take into account the magnetic saturation. The flux observer is also used to estimate the stator currents as well as to exclude a PLL for stator flux (or grid voltage) vector tracking needed for implementing vector control.

A new method for the identification of machine magnetizing characteristic is presented to get the saturation curve without traditional no-load tests of [17]. As opposed to [17], the method presented here does not require machine rotation and any additional instrumentation such as a power analyser. The available sensors are utilized for this test and the procedure is fully automatic. The identification scheme does not even need stator current measurement such that the procedure can also be carried out even in the absence of stator current sensors. The accuracy of the identified characteristic is compared with the one obtained through the standard procedure [17] and further verified by implementing DPC without stator current sensing.

The power control is implemented using an optimal voltage vector based modulated model predictive control (MPC). The modulated MPC optimizes the applied voltage vector both in linear regulation range as well as in over-modulation. The chosen MPC technique is particularly sensitive to machine parameters and it is selected to show that the identified magnetizing characteristic is accurate enough to allow a parameter-sensitive scheme to track power references accurately. The presented experimental results demonstrate that a fast dynamic performance is achieved even with a limited dc-link voltage. By using the identified machine magnetizing characteristic, almost zero steady state error in active and reactive power control can be obtained without measuring the stator current or when stator current sensing is unavailable due to a fault.

This article has been accepted for publication in a future issue of this journal, but has not been fully edited. Content may change prior to final publication. Citation information: DOI 10.1109/JESTPE.2020.3024679, IEEE Journal of Emerging and Selected Topics in Power Electronics

With respect to the available literature, the major contributions of the paper are:

1) **The MMPC with optimal voltage vector is applied, for the first time, for DPC of DFIM leading to the following benefits: (i) rapid transient response in linear regulation range and in over-modulation, (ii) constant switching frequency, (iii) power control even with limited dc-link voltage.**
2) **A novel method for magnetizing characteristic identification is presented and experimentally validated. The machine's saturation characteristic is identified at standstill, without requiring additional instrumentation, and with no stator current sensing. The identification method is fully automatic and is inherently position sensorless as no rotor position information is necessary.**
3) **Accurate reactive power estimation without stator current sensors is achieved by using the identified magnetizing characteristic that gives the accurate value of main inductance of the machine at various operating points.**
4) **For vector control, a PLL is completely excluded along with its shortcomings in terms of stability and tuning requirements. The flux-observer gives a reliable stator flux vector position information for field orientation.**
5) **It is shown that the sensors for stator current measurement can be excluded for cost reduction. Even if the current readings are necessary for power measurements, they can be obtained through low-cost devices without the need for high dynamic current sensors generally used for machine control.**

This work is a deeply revised version of [18] and has the following enhanements with respect to [18]:

- **A detailed description of the magnetizing characteristic identification method is given with experimental validation.**
- **The identified magnetizing characteristic is compared with the one obtained with a standard method [17] and a good match is observed.**
- **More experimental results are presented by using the identified magnetizing characteristic.**

The following sections briefly describe the modelling of a DFIM (section II) and the flux observer (section III) that does not need stator current measurement. In section IV a method for identifying the magnetizing characteristic of the machine is presented while section V details the modulated MPC strategy used in this paper. Section VI presents experimental results and, finally, section VII concludes the paper.

II. Modelling of DFIM for Direct Power Control

Like a squirrel cage induction machine, a DFIM consists of a distributed stator winding, but unlike a squirrel cage machine, the rotor of a DFIM also contains windings. These windings are connected to external circuit through slip rings. Fig. 1 shows a generalized scheme of DFIM connection to the grid. GSC stands for grid side converter and RSC for rotor side converter. The control of GSC is not discussed in this paper, the focus is on RSC control. It can be noticed that the stator current is not considered as a measured quantity.

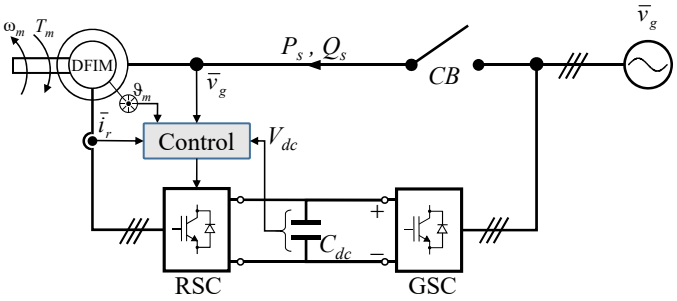

Fig. 1. Doubly-fed induction machine connection to the grid.

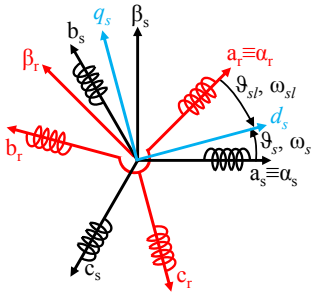

Fig. 2. DFIM reference frames definition.

A. Stator and rotor voltage equations

While writing the following equations, reference is made to Fig. 2 in which the reference frames are defined. The stator stationary reference frame $\alpha_s\beta_s$ has its α-axis aligned to phase 'a' of the stator winding. The reference frame $\alpha_r\beta_r$ is fixed with respect to the rotor windings and rotates at rotor angular speed ω_r (not shown in Fig. 2). The power control will be carried out in stator flux oriented (SFO) d_sq_s frame [19]. The stator and rotor voltage equations of a DFIM in stator flux-oriented (SFO) d_sq_s reference frame (defined in Fig. 2) can be written as:

$$\bar{v}_s = R_s\bar{i}_s + \frac{d\bar{\lambda}_s}{dt} + j\omega_s\bar{\lambda}_s \tag{1}$$

$$\bar{v}_r = R_r\bar{i}_r + \frac{d\bar{\lambda}_r}{dt} + j\omega_{sl}\bar{\lambda}_r \tag{2}$$

where $\bar{v}$, $\bar{i}$, $\bar{\lambda}$ are voltage, current and flux vectors, respectively, with subscript 's' denoting stator quantities while 'r' stands for rotor quantities. R_s and R_r are the stator and rotor resistance, respectively. ω_s is stator electrical frequency (in rad/s), ω_{sl} is the slip frequency (in rad/s) and j is the complex operator. The equations and parameters are referred to the stator side of the machine (for SFO control). The stator and rotor fluxes are related to respective currents through the following relations:

$$\bar{\lambda}_s = L_s\bar{i}_s + L_m\bar{i}_r \tag{3}$$

$$\bar{\lambda}_r = L_m\bar{i}_s + L_r\bar{i}_r \tag{4}$$

where L_s, L_r and L_m are stator, rotor and magnetizing inductance, respectively. It must be noted that (3) and (4) are valid

in all reference frames of Fig. 2, namely stator $\alpha_s\beta_s$, rotor $\alpha_r\beta_r$ and SFO d_sq_s frames.

Noting that the stator current $\bar{i}_s$ is not a measured quantity, it can be eliminated from the rotor flux equation by substituting (3) into (4) to get:

$$\bar{\lambda}_r = \sigma L_r \bar{i}_r + k_s \bar{\lambda}_s \tag{5}$$

where σ is the leakage factor defined as $1 - L_m^2/L_s/L_r$ and k_s is the stator coupling factor given by L_m/L_s. Substituting (5) into (2) and rearranging to obtain the rotor current state equation:

$$\frac{d\bar{i}_r}{dt} = -\frac{R_r}{\sigma L_r}\bar{i}_r - j\omega_{sl}\bar{i}_r - \frac{j\omega_{sl}k_s}{\sigma L_r}\bar{\lambda}_s + \frac{\bar{v}_r}{\sigma L_r} \tag{6}$$

B. Active and reactive power

The stator active and reactive power in terms of stator dq currents and voltages is given by:

$$P_s = \tfrac{3}{2}(v_{ds}i_{ds} + v_{qs}i_{qs}) \tag{7}$$

$$Q_s = \tfrac{3}{2}(v_{qs}i_{ds} - v_{ds}i_{qs}) \tag{8}$$

Since the active and reactive power control is achieved through rotor side, the stator currents in (7) and (8) can be replaced with rotor currents using (3).

$$\bar{i}_s = \frac{\bar{\lambda}_s - L_m\bar{i}_r}{L_s} \tag{9}$$

From the definition of SFO frame (of Fig. 2), it is noted that $\lambda_{ds} = |\bar{\lambda}_s|$ and $\lambda_{qs} = 0$. From (1), in steady state, the stator voltage is given by (10).

$$\bar{V}_s = R_s\bar{I}_s + j\omega_s\bar{\Lambda}_s \tag{10}$$

If $R_s|\bar{I}_s| \ll \omega_s|\bar{\Lambda}_s|$, then the stator voltage's dq components can be approximated as: $v_{qs} \approx |\bar{v}_g|$ and $v_{ds} \approx 0$, where $\bar{v}_g$ is the instantaneous grid voltage vector. Thus, after substituting (9) into (7) and (8), the stator active and reactive power in terms of grid voltage vector and rotor currents will be:

$$P_s = -\tfrac{3}{2}k_s|\bar{v}_g|i_{qr} \tag{11}$$

$$Q_s = \tfrac{3}{2}|\bar{v}_g|\left(\tfrac{|\bar{\lambda}_s|}{L_s} - k_s i_{dr}\right) \tag{12}$$

Taking the time derivative of (11) and (12) while noting that $|\bar{v}_g| = const.$ and $|\bar{\lambda}_s| = const.$ and substituting (6), the active and reactive power state equations become:

$$\tfrac{dP_s}{dt} = \tfrac{3}{2}k_s|\bar{v}_g|\left(\tfrac{R_r}{\sigma L_r}i_{qr} + \omega_{sl}i_{dr} + \tfrac{\omega_{sl}k_s}{\sigma L_r}|\bar{\lambda}_s| - \tfrac{v_{qr}}{\sigma L_r}\right) \tag{13}$$

$$\tfrac{dQ_s}{dt} = \tfrac{3}{2}k_s|\bar{v}_g|\left(\tfrac{R_r}{\sigma L_r}i_{dr} - \omega_{sl}i_{qr} - \tfrac{v_{dr}}{\sigma L_r}\right) \tag{14}$$

III. Flux Observer and Field Orientation

In order to get the measured quantities in SFO frame of Fig. 2, a PLL is generally used [10]. In this work, the full-state flux observer of an induction machine is exploited for field orientation. The flux-observer is constructed based on the stator and rotor voltage equations in respective stationary frames by setting $\omega_s = 0$ and $\omega_{sl} = 0$ in (1) and (2), respectively. The stator flux from the rotor and stator voltage equations (eliminating the stator current) is given in (15) and (16), respectively, where superscripts '*re*' and '*se*' stand for rotor equation and stator equation, respectively. In (16), τ_s represents stator time constant defined as L_s/R_s. It must be noted that $\bar{i}_r$ in (16) is the rotor current transformed to stator stationary frame $\alpha_s\beta_s$ of Fig. 2 through rotor mechanical angle θ_m.

$$\bar{\lambda}_s^{re} = \tfrac{1}{k_r}\left\{\int(\bar{v}_r - R_r\bar{i}_r)\,dt - \sigma L_r\bar{i}_r\right\} \tag{15}$$

$$\bar{\lambda}_s^{se} = \tfrac{1}{\tau_s}\left\{\int\left(-\bar{\lambda}_s + \tau_s\bar{v}_s + L_m\bar{i}_r\right)dt\right\} \tag{16}$$

A flux-observer is constructed by combining (15) and (16) through an observer gain g as shown in Fig. 3. This observer has the benefits of no open-loop integration as opposed to an observer based only on stator equation. To further mitigate the effects of dc-offset arising from grid voltage sensors, the pure integration of (16) is replaced with the scheme of [20]. In Fig. 3, the parameters such as L_m and τ_s are shown as functions of λ_m to appropriately consider their dependence on the saturation characteristic of the machine. Still in Fig. 3, Δ_{abc} represents the duty cycle vector of RSC switches, v_{dc} is the measured dc-link voltage and 'DT' stands for dead-time compensation LUTs [21], [22]. The inverter voltage error as a function of current ($\bar{v}_{\alpha\beta}^{dt}$) is subtracted from the applied voltage to obtain accurate rotor voltage for flux-observer.

The sine and cosine functions of stator flux angle are obtained directly from the α and β components of the observed flux as (17). The use of the flux-observer along with dc-offset elimination scheme [20] and inverter error compensation allows to replace the PLL altogether, with the stator frequency estimation given by (18).

$$\cos\hat{\theta}_s = \frac{\hat{\lambda}_{s\alpha}}{|\hat{\bar{\lambda}}_s|} \qquad \sin\hat{\theta}_s = \frac{\hat{\lambda}_{s\beta}}{|\hat{\bar{\lambda}}_s|} \tag{17}$$

$$\hat{\omega}_s = \frac{\hat{\lambda}_{s\alpha}\frac{d\hat{\lambda}_{s\beta}}{dt} - \hat{\lambda}_{s\beta}\frac{d\hat{\lambda}_{s\alpha}}{dt}}{|\hat{\lambda}_s|^2} \tag{18}$$

The other advantage of using the flux-observer of Fig. 3 is realized in terms of accurate stator current estimation that helps excluding the stator current sensors. The magnetizing characteristic of the machine is utilized to track online the change in magnetizing inductance L_m and, consequently, τ_s that gives accurate stator and rotor flux estimation from which the magnetizing flux-linkage $\bar{\lambda}_m$ is obtained using (19) that, in turn, gives estimated stator current through (20). In (19), L_{lr} denotes rotor leakage inductance.

$$\hat{\bar{\lambda}}_m = \hat{\bar{\lambda}}_r - L_{lr}\bar{i}_r \tag{19}$$

$$\hat{\bar{i}}_s = \frac{\hat{\bar{\lambda}}_m}{L_m\left(|\hat{\bar{\lambda}}_m|\right)} - \bar{i}_r \tag{20}$$

where $L_m(|\hat{\bar{\lambda}}_m|)$ signifies $L_m = f(|\hat{\bar{\lambda}}_m|)$ i.e. magnetizing inductance as a function of peak magnetizing flux.

IV. Magnetizing Characteristic Identification

It can be observed from (20) that the estimation accuracy of stator current depends on the correct value of the machine's magnetizing inductance L_m at a given operating point i.e. $|\bar{\lambda}_m|$. For a reliable estimate of stator current at all operating

This article has been accepted for publication in a future issue of this journal, but has not been fully edited. Content may change prior to final publication. Citation information: DOI 10.1109/JESTPE.2020.3024679, IEEE Journal of Emerging and Selected Topics in Power Electronics

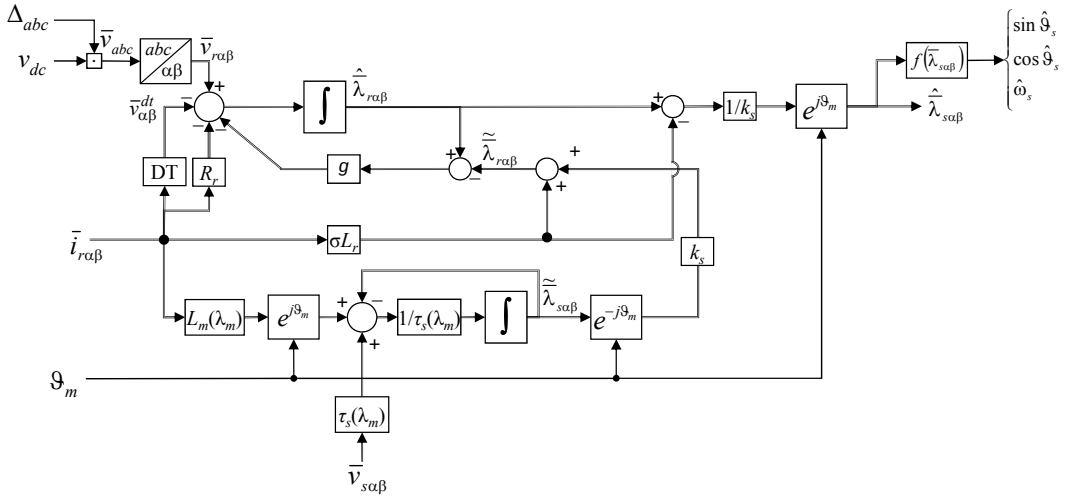

Fig. 3. Stator flux observer for DFIM.

conditions, the $L_m\left(|\bar{\lambda}_m|\right)$ curve must be known. This curve can be recovered from the magnetizing characteristic of the induction machine [23]. The standard method of identifying the magnetizing characteristic [17] may not be applicable when the machine is already installed and attached to the wind turbine. An alternate has to be found to identify this curve without requiring any additional sensors or additional equipment such as a wattmeter.

Benefiting from the possibility of accessing both stator and rotor windings of the machine, a test strategy can be devised for the identification of machine magnetizing curve. Looking at the diagram of Fig. 1, it can be seen that if the circuit breaker (CB) connecting the stator winding to the grid is open, the DFIM remains connected only to RSC while stator terminal voltage sensors still measure the voltage induced in the stator windings. If a current vector is established in the rotor windings through RSC and it is rotated, the voltage induced in the stator windings can be measured. The magnitude of current injected in the rotor can be increased up to the rated no-load current of the machine and the induced stator voltage measured and recorded for all rotor current values. The equivalent circuit of the machine for this test is as shown in Fig. 4.

Since the stator is in open-cricuit condition i.e. $\bar{i}_s = 0$, the measured stator voltage $\bar{v}_{s-meas}$ will correspond to the voltage across the magnetizing branch of the machine (see Fig. 4). In steady state, the stator voltage can be written from (1) and (3) as given in (21), where ω_{test} is the frequency at which the rotor current vector is rotated. Equivalently, the stator flux (or the main or mutual flux) can be obtained from (21) and expressed in (22).

$$\bar{V}_s = j\omega_{test} L_m \bar{I}_r \tag{21}$$

$$\bar{\Lambda}_s = \bar{\Lambda}_m = L_m \bar{I}_r \tag{22}$$

here, $\bar{\Lambda}_s$ and $\bar{\Lambda}_m$ represent stator and magnetizing flux linkage phasors (i.e. steady state quantities).

Since the stator voltage measured through voltage sensors does contain measurement noise and offset, the measured signal must first be filtered. However, simple low-pass filtering does not get rid of the offset, whose frequency is zero and therefore within the pass-band of the low-pass filter. A complex band-pass filter can be used with centre frequency tuned at ω_{test}. The filter's transfer function is given in (23) with ω_0 as its cut-off frequency. Of course, this filter requires two orthogonal signals at its input, so the implementation takes place in $\alpha\beta$ frame and not in phase quantities.

$$\bar{H}_{BPF} = \frac{\omega_{test}}{s - j\omega_0 + \omega_{test}} \tag{23}$$

Fig. 5 shows the results for a test carried out for magnetizing characteristic identification when a rotor current vector of 1A magnitude is rotated at 50Hz and the induced stator voltage is measured. The top plot shows rotor currents in rotor $\alpha\beta$ frame and the lower plot gives the induced stator voltage. The noise and offset in the measured voltage are effectively removed by the filter of (23) as seen in the figure. The filter's centre frequency is set as 50Hz (equal to that of the rotor current vector's rotation frequency) and its cut-off frequency is 20Hz. The filter of (23) does not introduce any phase delay even if the cut-off frequency of 20Hz is below that of the input signal (50Hz) thanks to the centre-frequency shift introduced through ω_{test}. In Fig. 6, a comparison between the magnetizing curve identified through the standard tests of [17] and through the

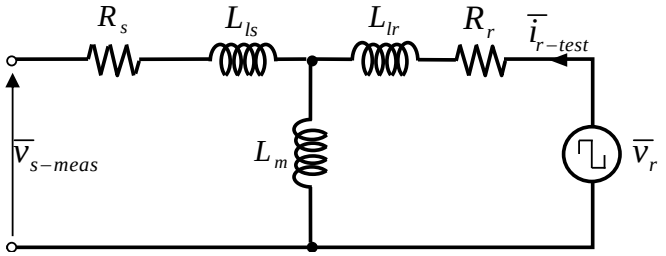

Fig. 4. Equivalent circuit for identification tests.

This article has been accepted for publication in a future issue of this journal, but has not been fully edited. Content may change prior to final publication. Citation information: DOI 10.1109/JESTPE.2020.3024679, IEEE Journal of Emerging and Selected Topics in Power Electronics

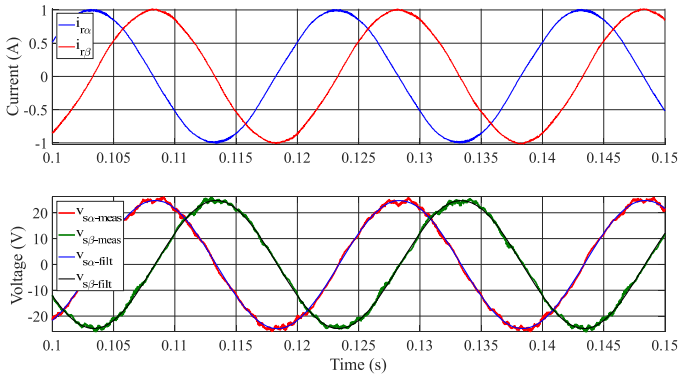

Fig. 5. Test results for magnetizing curve identification – top: rotor currents, bottom: stator induced voltages.

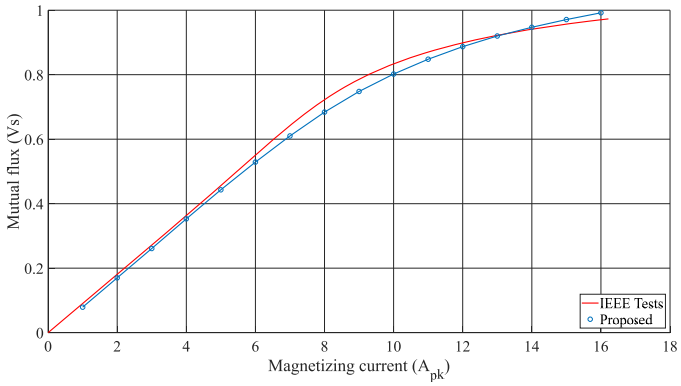

Fig. 6. Magnetizing curve comparison with standard tests.

proposed strategy is reported. It must be noted that the tests of [17] have some assumptions for the no-load condition; for instance the slip is assumed to be equal to zero in no-load when it is not entirely true. The test strategy proposed here does not require any such assumption and benefits from the added flexibility offered by the DFIM.

V. Modulated Model Predictive Control

In FCS-MPC, following a cost function minimization one of the seven possible inverter states are selected as optimal [24]. The selected inverter state is applied for a complete switching period. The FCS-MPC produces a variable switching frequency and gives higher ripple in controlled variables. In this paper, a modulated alternative of MPC is used based on [25], [26]. The application of any MPC scheme requires prediction of state variables. For this, the rotor current state equation (6) and the active and reactive power state equations (13) and (14) are discretized using Euler's approximation as follows, where k denotes current sampling instant and $k+1$ the next and T_s is the sampling time. Even though the grid voltage $\bar{v}_g$, the stator flux $\bar{\lambda}_s$ and the slip frequency ω_{sl} do not vary much over one sampling interval, they are written with sampling instant markers k, $k-1$ for correctness.

$$\bar{i}_r(k) = \left(1 - \frac{R_r T_s}{\sigma L_r}\right)\bar{i}_r(k-1) - j\omega_{sl}(k-1)\,T_s\bar{i}_r(k-1) - \frac{j\omega_{sl}(k-1)\,k_s}{\sigma L_r}T_s\bar{\lambda}_s(k-1) + \frac{T_s}{\sigma L_r}\bar{v}_r(k-1) \quad (24)$$

$$P_s(k+1) = P_s(k) + \frac{3}{2}T_s k_s|\bar{v}_g(k)|\left\{\frac{R_r}{\sigma L_r}i_{qr}(k) + \omega_{sl}(k)\,i_{dr}(k) + \frac{\omega_{sl}(k)\,k_s}{\sigma L_r}|\bar{\lambda}_s(k)| - \frac{v_{qr}(k)}{\sigma L_r}\right\} \quad (25)$$

$$Q_s(k+1) = Q_s(k) + \frac{3}{2}T_s k_s|\bar{v}_g(k)|\left\{\frac{R_r}{\sigma L_r}i_{dr}(k) - \omega_{sl}(k)\,i_{qr}(k) - \frac{v_{dr}(k)}{\sigma L_r}\right\} \quad (26)$$

Fig. 7 gives the flowchart of the control algorithm that proceeds in the following sequence:

- The grid voltage $\bar{v}_g$ and rotor current $\bar{i}_r$ are read in stator and rotor reference frames, respectively. The rotor mechanical position is acquired from the rotor position sensor.
- The flux-observer of Fig. 3 estimates the stator flux ($\bar{\lambda}_s$) and gives the sine and cosine of stator flux angle.
- The measured stator voltages and rotor currents are transformed to d_sq_s-frame.
- The rotor current vector is predicted using (24) based on the measurements and the applied rotor voltage $\bar{v}_r$ at previous sampling instant (after removing the inverter dead-time effects for accurate prediction).
- The stator active and reactive power at the current sampling instant is obtained using (11) and (12).
- To obtain predictions for the next sampling instant, every inverter switching state is evaluated. The voltage vector in rotor $\alpha_r\beta_r$ frame is given by (27) for different switching states.

$$\bar{v}_{\alpha\beta r} = \frac{2}{3}v_{dc}\begin{bmatrix}1 & e^{j\frac{2\pi}{3}} & e^{j\frac{-2\pi}{3}}\end{bmatrix}\begin{bmatrix}S_a\\S_b\\S_c\end{bmatrix} \quad (27)$$

where S denotes switching function with subscripts 'a', 'b', and 'c' representing phases. The top switch of the inverter leg is closed for $S=1$.

- The voltage vector of (27) is converted to SFO dq-frame for each of the seven inverter states and the active and reactive power for the next sampling instant are predicted through (25) and (26).
- An error vector is computed based on the reference values of active and reactive power as:

$$\bar{e}_i = (P_s^* - P_s(k+1)) + j(Q_s^* - Q_s(k+1)) \quad (28)$$

where the subscript 'i' denotes the inverter state $i \in [0,1,...,6]$ with $\bar{e}_0$ denoting the error when zero vector is applied.

- The two inverter states that are adjacent and that give minimum magnitude of the error vector (28) are identified [26].

This article has been accepted for publication in a future issue of this journal, but has not been fully edited. Content may change prior to final publication. Citation information: DOI 10.1109/JESTPE.2020.3024679, IEEE Journal of Emerging and Selected Topics in Power Electronics

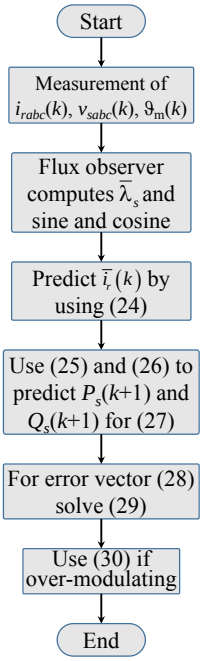

Fig. 7. Flowchart of the control sequence.

- The following system of linear equations is solved to compute the duty cycle d_1 and d_2 of each of the two vectors identified in the previous step [25].

$$\begin{bmatrix} e_{1P}-e_{0P} & e_{2P}-e_{0P} \\ e_{1Q}-e_{0Q} & e_{2Q}-e_{0Q} \end{bmatrix} \begin{bmatrix} d_1 \\ d_2 \end{bmatrix} = \begin{bmatrix} -e_{0P} \\ -e_{0Q} \end{bmatrix} \tag{29}$$

  Here, the subscripts 'P' and 'Q' denote the real and imaginary parts of the error vector $\bar{e}_i$, respectively.
- When the target active (P_s^*) and reactive (Q_s^*) power is achievable in one switching period, the duty cycles given by (29) satisfy $d_1+d_2 \leq 1$ and the duty cycle for zero vector is obtained as $d_0 = 1-d_1-d_2$. This is the linear regulation regime.
- The over-modulation region is encountered when the target active and reactive power cannot be reached in one switching period. In that case the solution of (29) produces the condition $d_1+d_2 > 1$. In order to maintain optimality also in case of over-modulation, the duty cycles are linearly scaled down as:

$$d_1 = \frac{d_1}{d_1+d_2}, \qquad d_2 = 1-d_1, \qquad d_0 = 0 \tag{30}$$

VI. Experimental Validation

The validation of the proposed direct power control strategy through modulated MPC is carried out on a commercial 7.5 kW wound rotor induction machine with its rotor windings accessible through slip rings. Fig. 8 shows the overall control block diagram with various measurements. The GSC of Fig. 1 is not shown in the diagram; it is assumed that the dc-link voltage is maintained by an external source for simplicity. The simulation results can be found in [18]. The machine's main inductance as a function of magnetizing current is first identified through the tests presented in section IV. The

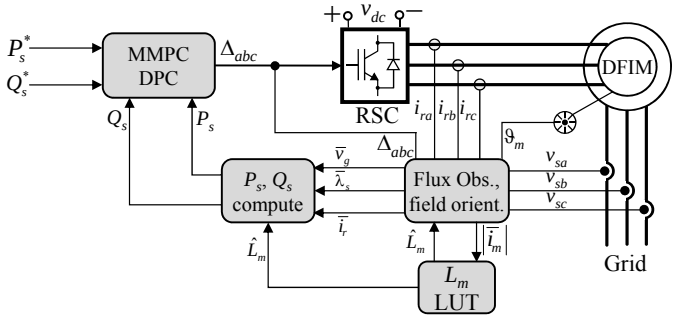

Fig. 8. Overall control block diagram.

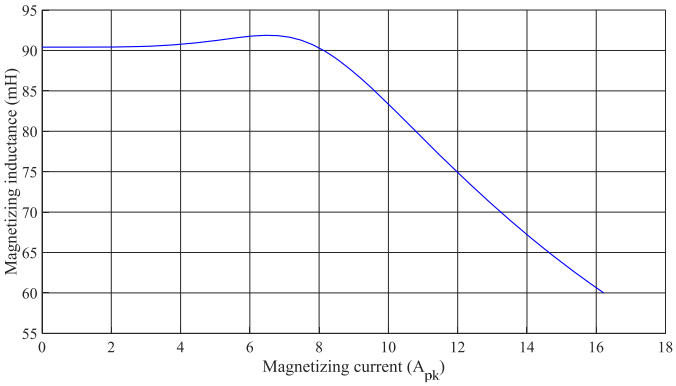

Fig. 9. Main inductance as a function of peak magnetizing current.

variation in magnetizing inductance as a function of current is reported in Fig. 9.

It can be observed that in deep saturation, the magnetizing inductance reduces by about a third which has major implications on reactive power estimation using (12) if stator currents are not measured. Other equivalent circuit parameters identified for the test machine are: $R_s = 0.41\ \Omega$, $R_r = 0.31\ \Omega$, $L_{ls} = L_{lr} = 5.7$ mH. In Fig. 3, the observer gain g (in rad/s) decides the frequency at which to swtich between the stator and rotor equations. With the magnetizing inductance accurately tracked from Fig. 9, it is safe to use stator equation for all operating frequencies normally encountered in a DFIM operation. Therefore, the value of g is set as high as $2\pi \cdot 2000$ rad/s.

Fig. 10 shows the photo of the test rig where the DFIM is coupled with a permanent-magnet synchronous machine that acts as a prime mover. The rotor position for the DFIM is obtained through a 25000 pulse per revolution incremental encoder. The stator voltage and current measurements are made available through appropriate voltage and current sensors. It must be noted that the stator current measurement is used only for verification purposes.

The RSC is a commercial 2 kW drive whose control board is replaced to allow direct access to the insulated gate bipolar transistors' (IGBT) gate drivers. The control algorithm runs on a custom DSP/FPGA board [27] that sends the switch duty cycle commands over a fibre-optic link. The fibre-optic interface ensures electrical isolation between the control platform and the power board of the commercial drive. The

This article has been accepted for publication in a future issue of this journal, but has not been fully edited. Content may change prior to final publication. Citation information: DOI 10.1109/JESTPE.2020.3024679, IEEE Journal of Emerging and Selected Topics in Power Electronics

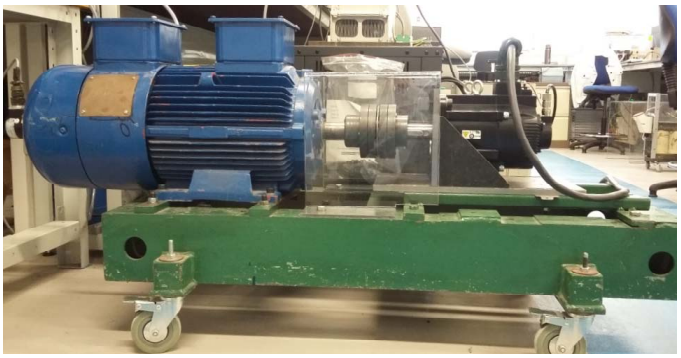

Fig. 10. Experimental setup – left: DFIM under test, right: prime mover.

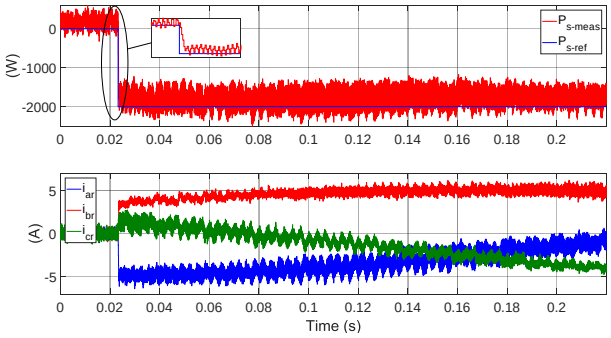

Fig. 11. Experimental results for active power step response – top: reference and measured active power, bottom: measured rotor phase currents.

switching frequency is 10 kHz. The shaft speed is maintained through the prime mover. The stator is connected to a 50 Hz grid.

A. Active and reactive power step response

Fig. 11 shows the results for an active power reference step of 2 kW when the shaft speed is maintained at 1540 rpm. The lower plot shows the rotor phase currents. It must be noted that the convention of consumer is used for the sign of power i.e. positive power is drawn from the grid and negative is injected into it. Fig. 12 gives the results for reactive power control. For this test, the shaft speed is reduced to 1500 rpm such that no active power is produced/consumed. The stator no-load reactive power at rated flux is close to 5000 VAr which is brought to 0 VAr to effectuate unity power factor operation. The lower plot of the figure shows the d- and q-axis stator currents. The stator d-axis current at no-load is the rated magnetizing current (see Fig. 6 and Fig. 9) which is compensated through the rotor circuit that results in unity power factor operation (of the stator circuit). The inset graphs in Fig. 11 and Fig. 12 show the zoomed-in results for control dynamics. It must be noted that to obtain the results of Fig. 11 and Fig. 12, the measured stator current is used only to compute active (P_{s-meas}) and reactive (Q_{s-meas}) power but the control and flux-observer do not include stator current measurement. Instead, the LUT (of Fig. 9) is used to correct L_m online based on the observed mutual flux value.

Fig. 13 presents results for a step change in both active and reactive power at the same instant ($\omega_m = 1540$ rpm). It

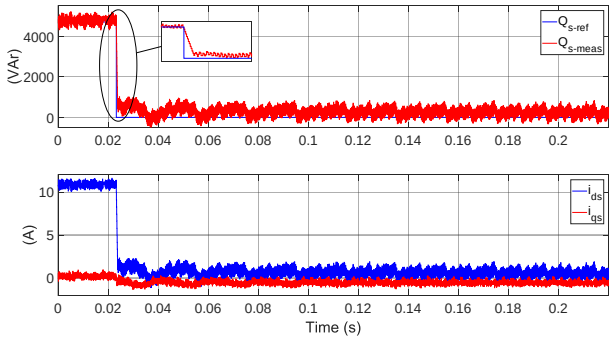

Fig. 12. Experimental results for reactive power step response – top: reference and measured reactive power, bottom: measured stator d- and q-axis currents.

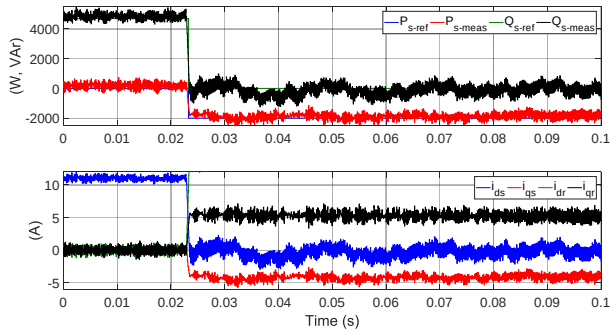

Fig. 13. Experimental results for active and reactive power step response – top: reference and measured power, bottom: measured stator and rotor d- and q-axis currents.

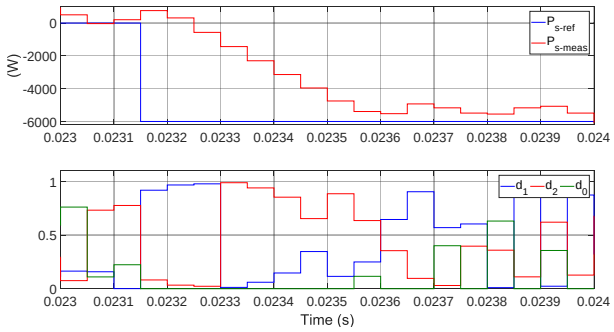

Fig. 14. Experimental results for active power step for overmodulation – top: reference and measured active power, bottom: duty cycles given by (29) and (30).

can be observed that the control dynamics of Fig. 11 and Fig. 12 are preserved. The stator and rotor d- and q-axis currents are also reported for completeness. Furthermore, to verify the operation in overmodulation region, an active power step of 6 kW (80% of rated machine power) is applied and the duty cycles given by (29) and (30) are shown in Fig. 14. The figure is zoomed in around the instant when the step is applied to show saturated operation for initial instants (notice that $d_0 = 0$) and the modulation once the target is achievable in one switching instant (now $d_0 \neq 0$).

B. Saturation influence on reactive power

To demonstrate that in the absence of stator current measurement, the reactive power control is affected by whether

This article has been accepted for publication in a future issue of this journal, but has not been fully edited. Content may change prior to final publication. Citation information: DOI 10.1109/JESTPE.2020.3024679, IEEE Journal of Emerging and Selected Topics in Power Electronics

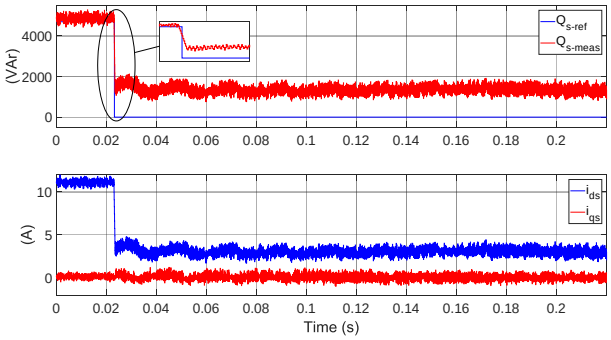

Fig. 15. Experimental results for reactive power step response with constant L_m – top: reference and measured reactive power, bottom: measured stator d- and q-axis currents.

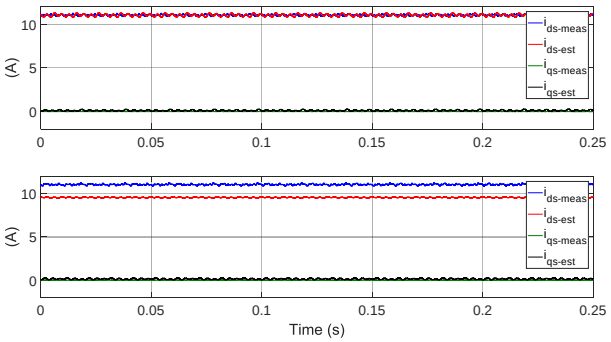

Fig. 16. Experimental results for stator d- and q-axis current estimation – top: measured and estimated currents with LUT, bottom: measured and estimated currents with constant L_m.

the saturation characteristic (Fig. 6 and Fig. 9) is taken into account or not, the reactive power step test of Fig. 12 is repeated but without LUT for L_m correction. The result presented in Fig. 15 shows that the reactive power control has a considerable steady-state error and the same is noted from the stator d-axis current (shown in the lower plot). All other conditions of Fig. 12 are kept the same for Fig. 15.

Since the stator current estimation, particularly the d-axis current, influences the estimation accuracy of the reactive power through (8), the measured and estimated stator current components are compared next. The stator current estimated through (20) is compared with the measured current in Fig. 16. The top plot shows the comparison when the LUT of Fig. 9 is used for L_m correction. The bottom plot shows the estimate with constant L_m. It is evident that the stator current estimation (especially i_{ds}) is significantly improved with the LUT. Fig. 16 also confirms that, with the proposed method, a continuous direct power control operation without steady-state error on reactive power can be guaranteed in the event of stator current sensor failure (see also Fig. 12 and 15).

Whereas the reactive power is sensitive to saturation effects, the active power control does not suffer from this. The active power control results given in Fig. 17 show that with constant L_m the estimate of active power has no error and therefore the steady state error is limited (as in Fig. 11).

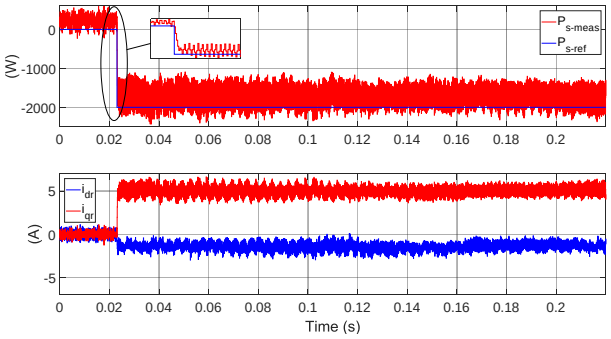

Fig. 17. Experimental results for active power step response with constant L_m – top: reference and measured active power, bottom: measured rotor d- and q-axis currents.

VII. Conclusions

In this paper, a model predictive control strategy based on optimal voltage vectors is applied for direct power control of a DFIM. The paper has focused on the magnetic saturation effects that influence the estimation, and therefore the control, of reactive power in the absence of stator current measurement. It has been shown that if the magnetizing characteristic of the machine is known, the reactive power control with null steady state error is possible even in the event of stator current sensor failure, which helps improve the fault-tolerance. A new self-commissioning method for on-site identification of the magnetizing characteristic is also presented and verified experimentally. A flux observer is designed starting from the measured electrical quantities and, thanks to this flux observer, the need for a phase-locked loop is also eliminated for field orientation. The experimental results have demonstrated that an open-loop reactive power control can be achieved without significant steady-state error in the absence of stator current measurement. In this work, the rotor position is measured through an incremental encoder, the implementation of the presented self-commissioning method and control strategy for a rotor position sensorless control will be part of future research in this direction.

References

[1] B. Mecrow and A. Jack, "Efficiency trends in electric machines and drives," *Energy Policy*, vol. 36, no. 12, pp. 4336 – 4341, 2008, foresight Sustainable Energy Management and the Built Environment Project.

[2] D. Phares, T. Ruegg, and K. Fishel, "Energy-Saving Project of 5500-HP 13-kV Wound Rotor Induction Motor on a Kiln ID Fan Using a Low-Voltage Slip Power Recovery Drive – A Case Study," *IEEE Trans. Ind. Appl.*, vol. 53, no. 6, pp. 5997–6001, Nov. 2017.

[3] J. Hu, J. Zhu, Y. Zhang, G. Platt, Q. Ma, and D. G. Dorrell, "Predictive direct virtual torque and power control of doubly fed induction generators for fast and smooth grid synchronization and flexible power regulation," *IEEE Trans. Power Electron.*, vol. 28, no. 7, pp. 3182–3194, 2013.

[4] D. Zhi, L. Xu, and B. W. Williams, "Model-Based Predictive Direct Power Control of Doubly Fed Induction Generators," *IEEE Trans. Power Electron.*, vol. 25, no. 2, pp. 341–351, 2010.

[5] R. Datta and V. Ranganathan, "Direct power control of grid-connected wound rotor induction machine without rotor position sensors," *IEEE Trans. Power Electron.*, vol. 16, no. 3, pp. 390–399, May 2001.

[6] D. Sun, X. Wang, H. Nian, and Z. Zhu, "A Sliding-Mode Direct Power Control Strategy for DFIG Under Both Balanced and Unbalanced Grid Conditions Using Extended Active Power," *IEEE Trans. Power Electron.*, vol. 33, no. 2, pp. 1313–1322, 2018.

[7] H. Nian and L. Li, "Direct Power Control of Doubly Fed Induction Generator Without Phase-Locked Loop Under Harmonically Distorted Voltage Conditions," *IEEE Trans. Power Electron.*, vol. 33, no. 7, pp. 5836–5846, Jul. 2018.

[8] M. E. Zarei, C. V. Nicolás, and J. R. Arribas, "Improved Predictive Direct Power Control of Doubly Fed Induction Generator during Unbalanced Grid Voltage Based on Four Vectors," *IEEE J. Emerg. Sel. Topics Power Electron.*, vol. 5, no. 2, pp. 695–707, 2017.

[9] M. P. Kazmierkowski, L. G. Franquelo, J. Rodriguez, M. A. Perez, and J. I. Leon, "High-performance motor drives," *IEEE Industrial Electronics Magazine*, vol. 5, no. 3, pp. 6–26, 2011.

[10] A. J. S. Filho, A. L. Oliveira, L. L. Rodrigues, E. C. M. Costa, and R. V. Jacomini, "A robust finite control set applied to the DFIG power control," *IEEE J. Emerg. Sel. Topics Power Electron.*, pp. 1–1, 2018.

[11] J. Hu, J. Zhu, and D. G. Dorrell, "Predictive Direct Power Control of Doubly Fed Induction Generators Under Unbalanced Grid Voltage Conditions for Power Quality Improvement," *IEEE Trans. Sustain. Energy*, vol. 6, no. 3, pp. 943–950, 2015.

[12] H. T. Nguyen, E.-K. Kim, I.-P. Kim, H. H. Choi, and J.-W. Jung, "Model Predictive Control with Modulated Optimal Vector for a Three-Phase Inverter with an LC filter," *IEEE Trans. Power Electron.*, vol. 33, no. 3, pp. 2690–2703, 2018.

[13] C. Dirscherl and C. M. Hackl, "Model predictive current control with analytical solution and integral error feedback of doubly-fed induction generators with LC filter," in *2017 IEEE Int. Symp. Predictive Control of Elect. Drives and Power Electron. (PRECEDE)*. IEEE, Sep. 2017, pp. 25–30.

[14] R. Peña, R. Cárdenas, E. Reyes, J. Clare, and P. Wheeler, "Control of a Doubly Fed Induction Generator via an Indirect Matrix Converter With Changing DC Voltage," *IEEE Trans. Ind. Electron.*, vol. 58, no. 10, pp. 4664–4674, 2011.

[15] N. Amiri, S. M. Madani, T. A. Lipo, and H. A. Zarchi, "An improved direct decoupled power control of doubly fed induction machine without rotor position sensor and with robustness to parameter variation," *IEEE Trans. Energy Convers.*, vol. 27, no. 4, pp. 873–884, 2012.

[16] D. F. Howard, L. Jiaqi, and R. G. Harley, "Short-circuit modeling of DFIGs with uninterrupted control," *IEEE J. Emerg. Sel. Topics Power Electron.*, vol. 2, no. 1, pp. 47–57, 2014.

[17] IEEE, "IEEE Standard Test Procedure for Polyphase Induction Motors and Generators," pp. 1–79, 2004.

[18] S. Odhano, S. Rubino, P. Zanchetta, and R. Bojoi, "Modulated Model Predictive Direct Power Control of DFIM Considering Magnetic Saturation Effects," in *Proceedings - IEEE Energy Conversion Congress and Exposition (ECCE-2018)*, Portland, Sep. 2018, pp. 5442–5449.

[19] G. Abad, J. Lopez, M. A. Rodriguez, L. Marroyo, and G. Iwanski, *Doubly Fed Induction Machine*. New Jersey: Wiley, 2011.

[20] D. Stojic, M. Milinkovic, S. Veinovic, and I. Klasnic, "Improved Stator Flux Estimator for Speed Sensorless Induction Motor Drives," *IEEE Trans. Power Electron.*, vol. 30, no. 4, pp. 2363–2371, Apr. 2015.

[21] S. Odhano, M. Tang, A. Formentini, P. Zanchetta, and R. Bojoi, "Identification of Linear Permanent Magnet Synchronous Motor Parameters and Inverter Non-Linearity Effects," in *2018 International Symposium on Power Electronics, Electrical Drives, Automation and Motion (SPEEDAM)*, Jun. 2018, pp. 26–32.

[22] G. Pellegrino, R. I. Bojoi, P. Guglielmi, and F. Cupertino, "Accurate Inverter Error Compensation and Related Self-Commissioning Scheme in Sensorless Induction Motor Drives," *IEEE Trans. Ind. Appl.*, vol. 46, no. 5, pp. 1970–1978, Sep. 2010.

[23] S. Odhano, A. Cavagnino, R. Bojoi, and A. Tenconi, "Induction motor magnetizing characteristic identification at standstill with single-phase tests conducted through the inverter," in *Proceedings - 2015 IEEE International Electric Machines and Drives Conference, IEMDC 2015*, 2015.

[24] J. Rodriguez, M. P. Kazmierkowski, J. R. Espinoza, P. Zanchetta, H. Abu-Rub, H. A. Young, and C. A. Rojas, "State of the Art of Finite Control Set Model Predictive Control in Power Electron." *IEEE Trans. Ind. Informat.*, vol. 9, no. 2, pp. 1003–1016, May 2013.

[25] E. Fuentes, C. A. Silva, and R. M. Kennel, "MPC Implementation of a Quasi-Time-Optimal Speed Control for a PMSM Drive, With Inner Modulated-FS-MPC Torque Control," *IEEE Trans. Ind. Electron.*, vol. 63, no. 6, pp. 3897–3905, Jun. 2016.

[26] C. F. Garcia, C. A. Silva, J. R. Rodriguez, P. Zanchetta, and S. A. Odhano, "Modulated Model Predictive Control with Optimized Overmodulation," *IEEE J. Emerg. Sel. Topics Power Electron.*, pp. 1–1, 2018.

[27] A. Galassini, G. Lo Calzo, A. Formentini, C. Gerada, P. Zanchetta, and A. Costabeber, "ucube: Control platform for power electronics," in *2017 IEEE Workshop on Electrical Machines Design, Control and Diagnosis (WEMDCD)*, 2017, pp. 216–221.